IOP Publishing Physica Scripta
Phys. Scr. 95 (2020) 045603 (9pp) https://doi.org/10.1088/1402-4896/ab5bbd

Electrostatic solitary pulses in magnetized relativistic spin-polarized quantum plasma

Nabi Gul, Ikramullah, Rashid Ahmad, Muhammad Adnan and Fida Younus Khattak

Department of Physics, Kohat University of Science and Technology, Kohat 26000, Khyber Pakhtunkhwa, Pakistan

E-mail: fida@kust.edu.pk

Received 20 September 2019, revised 14 November 2019
Accepted for publication 26 November 2019
Published 12 February 2020

Abstract

A *Magnetized Relativistic Quantum Hydrodynamics* model is used to study the behavior of low fRequency electrostatic solitons in relativistic magnetized spin-polarized quantum plasma. The constituents of the plasma are inertia-less relativistic quantum electrons having concentration of both spin-up $n_{e\uparrow}$ and spin-down $n_{e\downarrow}$ species, and relativistic classical ions. We have used two-dimensional geometry in which a uniform ambient magnetic field is applied in the z-direction i.e. $\mathbf{B} = B_0\hat{z}$. The linear analysis shows the presence of two types of modes; slow (acoustic) mode and a fast *Langmuir*-like mode. A nonlinear Zakharov–Kuznetsov (ZK) type equation is derived for the electrostatic potential by using reductive perturbation technique. The dependence of the spin density polarization ratio κ on the properties of solitary wave profile is being investigated. It has been demonstrated that amplitude as well as width of the soliton depend significantly on the spin density polarization ratio, obliqueness and relativistic effects. We have also observed that the soliton solution of the ZK equation is unstable to the oblique perturbations. The instability growth rate varies appreciably with the density polarization and relativistic effects.

Keywords: solitary structures, relatvistic plasma, spin polarized plasma, magnetized plasma, quantum plasma

(Some figures may appear in colour only in the online journal)

1. Introduction

At extremely high density and low temperature, the *de Broglie* wavelength of the constituent particles of plasma becomes comparable to the mean distance between the particles and the wavefunctions start to overlap. These systems are commonly referred to as quantum plasmas as the quantum nature of particles in such a system affects the entire dynamics. Such plasmas can be observed in astrophysical objects [1–3], miniature semiconducting devices [4], metallic nano-structures [5], inertial confinement fusion experiments [6], etc. Quantum properties have already been experimentally observed and measured in a laser generated beryllium plasma [7]. Many researchers have theoretically investigated various aspects of quantum plasmas, see for example [8–11] and many references therein. Our motivation for this work stems from the developments in short- pulse high-power laser technology (see for example [12]) that has made the generation of such plasmas possible in a laboratory environment.

If the average energy contents of the constituent particles exceed their rest mass energy, relativistic effects will become important as the relativistic parameter P_f/mc [13] will have an appreciable magnitude and could not be ignored. Here P_f and m are respectively the *Fermi* momentum and mass of the constituent particle and c is the speed of light in free space. In compact interstellar objects where the particle number density can be of the order of $10^{30}\,\mathrm{cm}^{-3}$ (white dwarf) or even $10^{36}\,\mathrm{cm}^{-3}$ (neutron star), Chandrasekhar [14, 15] has mathematically explained the equation of state for such systems for two limits, non-relativistic and ultra-relativistic limit. If the *Fermi* energy of the constituent particles of quantum plasma is too large compared to its thermal energy, the plasma is considered as cold i.e. carrying zero kinetic temperature even if it is of the order 10^9 K [16]. Mc kerr *et al* [17] have developed a

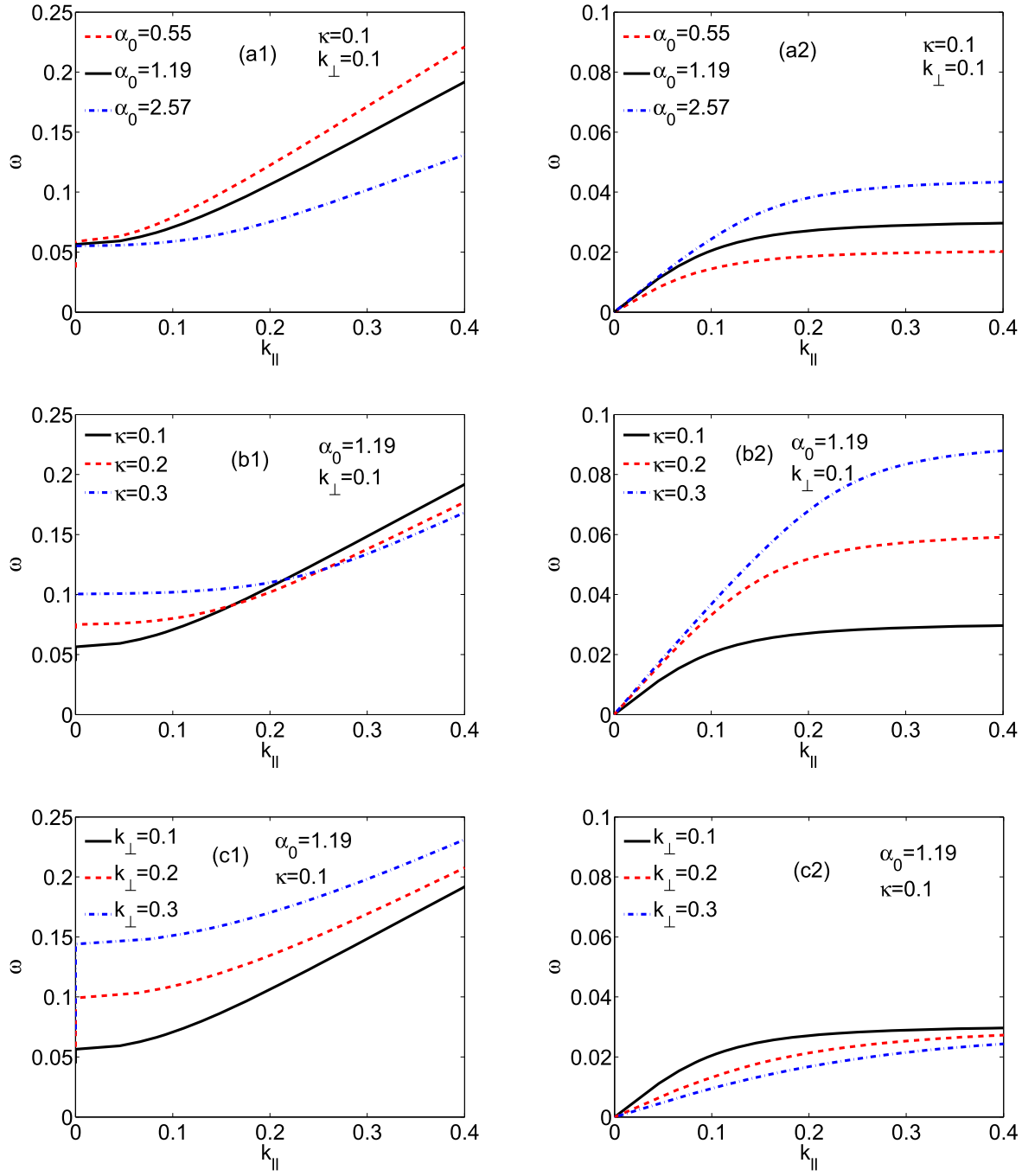

Figure 1. Plots showing normalized angular frequency ω (normalized by ω_{pi}) versus parallel propagation vector $k_{\|}$ (normalized by λ_i). The left side graphs depict the high frequency modes while the right side plots show the low frequency modes. The top two plots (a1) and (a2) show how the relativistic factor affects these two modes by plotting the frequency against the parallel wave vector for three different cases, weakly relativistic, relativistic and ultra-relativistic. In these cases, $k_{\perp} = 0.1$ and $\kappa = 0.1$. The middle plots (b1) and (b2) show the spin polarization effect on the dispersion for a relativistic case at $k_{\perp} = 0.1$. The bottom plots (c1) and (c2) show the effect of variation of the perpendicular component of the wave vector $k_{\perp}$ (signifying obliqueness) for the relativistic case while keeping $\kappa = 0.1$.

relativistic two fluid model and studied relativistic solitary structure by assuming one dimensional geometry. The propagation of electrostatic solitary pulses has also been investigated in a relativistic and magnetized quantum plasma by applying a quantum hydrodynamic model [11].

Quantum plasmas obey *Fermi–Dirac* statistics as the *Pauli Exclusion Principle* does not allow electrons to occupy the same state due to its identical nature. Contrary to the classical thermal pressure, the *Fermi* pressure does not vanish at low temperature. Furthermore, *Bohm* potential and particle spin are the other important effects associated with quantum plasma that are to be incorporated in the fluid modeling of the system. The *Bohm* potential enters through the density perturbations while the spin effects associated with intrinsic spin magnetic moment of the plasma species can be introduced in the equation of motion through the magnetization energy. A detailed description of

modeling quantum plasma is discussed by Manfredi [18] wherein different plasma models (kinetic and fluid) are used to investigate the collective properties of degenerate plasma.

Brodin *et al* [19] presented a review of different mathematical models to study magnetization effects produced due to electron spin angular momentum in quantum plasma. Andreev and Kuz'menkov [20] studied oblique propagation of *longitudinal waves in magnetized spin-1/2 plasmas* considering spin-up and spin-down electrons as two different populations. They have observed additional modes during oblique propagation of longitudinal waves in magnetized quantum plasmas. Furthermore, Andreev [10] has given a brief and comprehensive study of separated spin degenerate electrons and has observed the existence of spin-electron acoustic wave. Recently, the spin polarization effects on the characteristic profile of electrostatic solitary structure and on the instability of the soliton to obliquely propagating perturbations have been studied in [21].

In this article, we examine the propagation of electrostatic solitary structures in relativistic quantum plasmas consisting of relativistic inertia-less quantum electrons having both spin-up ($n_{e\uparrow}$) and spin-down ($n_{e\downarrow}$) concentrations and classical relativistic ions by using the approach developed in [11]. By using the standard analytical approach called reductive perturbation technique (RPT), a nonlinear differential equation of *Zakharov–Kuznetsov* (ZK) type is obtained to study the propagation of solitary structures. It has been observed that the solitons are not stable to oblique propagation. We investigate anaytically the dependence of the instability growth rate on various plasma parameters. In section 2, we present a mathematical model governing the low frequency (ion-scale) electrostatic perturbations in magnetized relativistic quantum plasma composed of relativistic inertia-less degenerate electrons of spin-up ($n_{e\uparrow}$) and spin-down ($n_{e\downarrow}$) concentrations and relativistic classical ions. Section 3 describes the linear properties of such system. The ion-acoustic waves (IAWs) propagation is studied in section 4 by deriving a nonlinear evolution equation (ZK-type). An explanation of soliton solution is given in its subsection. The results are discussed thoroughly by varying various plasma parameters. The stability of oblique propagation of solitons is investigated in section 5. We conclude our work in section 6.

2. Mathematical model

We use a *magnetized relativistic quantum hydrodynamics* (MRQH) model to study relativistic quantum plasma composed of relativistic inertia-less quantum electrons, both spin up ($n_{e\uparrow}$) and spin down ($n_{e\downarrow}$), and relativistic classical ions [10, 11]. We have used a two-dimensional configuration and have assumed the evolution and propagation of plasma excitations in the *X*–*Z*-plane. Therefore, we will take $\nabla = (\partial_x, 0, \partial_z)$. A uniform ambient magnetic field is applied in the z-direction i.e. $\mathbf{B} = B_0\hat{z}$. The dynamics of classical relativistic ions is governed by the following set of equations:

$$\frac{\partial(\gamma_i n_i)}{\partial t} + \nabla \cdot (\gamma_i n_i \mathbf{v}_i) = 0, \tag{1}$$

$$\left(\frac{\partial}{\partial t} + \mathbf{v}_i \cdot \nabla\right)\gamma_i \mathbf{v}_i = \frac{e}{m_i}\mathbf{E} + \frac{eB_0}{m_i c}\mathbf{v}_i \times \hat{z}. \tag{2}$$

The set of equations (continuity and momentum equations) describing the dynamics of spin-up ($n_{e\uparrow}$) and spin-down ($n_{e\downarrow}$) inertia-less relativistic degenerate electrons are:

$$\frac{\partial(\gamma_\uparrow n_{e\uparrow})}{\partial t} + \nabla \cdot (\gamma_\uparrow n_{e\uparrow} \mathbf{v}_{e\uparrow}) = 0, \tag{3}$$

$$\frac{\partial(\gamma_\downarrow n_{e\downarrow})}{\partial t} + \nabla \cdot (\gamma_\downarrow n_{e\downarrow} \mathbf{v}_{e\downarrow}) = 0, \tag{4}$$

$$0 = -en_\uparrow\left(\mathbf{E} + \frac{B_0}{c}\mathbf{v}_{e\uparrow} \times \hat{z}\right) - \frac{m_e c^2 \gamma_\uparrow}{P_{e\uparrow} + \rho_e}\left(\nabla + \frac{\mathbf{v}_{e\uparrow}}{c^2}\frac{\partial}{\partial t}\right)P_{e\uparrow}, \tag{5}$$

$$0 = -en_\downarrow\left(\mathbf{E} + \frac{B_0}{c}\mathbf{v}_{e\downarrow} \times \hat{z}\right) - \frac{m_e c^2 \gamma_\downarrow}{P_{e\downarrow} + \rho_e}\left(\nabla + \frac{\mathbf{v}_{e\downarrow}}{c^2}\frac{\partial}{\partial t}\right)P_{e\downarrow}. \tag{6}$$

The *Poisson* equation which closes the system of equations is given as:

$$\nabla \cdot \mathbf{E} = 4\pi e(\gamma_i n_i - \gamma_\downarrow n_{e\downarrow} - \gamma_\uparrow n_{e\uparrow}). \tag{7}$$

The electric field is defined in terms of electrostatic potential ϕ as $\mathbf{E} = -\nabla\phi$, $\gamma_{i,\uparrow,\downarrow} = \sqrt{1 - v_{i,\uparrow,\downarrow}^2/c^2}$ is the gamma factor describing the relativistic effects. Here the subscripts i.e. represent ion and electron respectively. The relativistic degenerate pressure P_{es} of spin-up ($n_{e\uparrow}$) and spin-down ($n_{e\downarrow}$) degenerate electrons is given by:

$$P_{es} = \frac{m^4 c^5}{24\pi^2\hbar^3}(\alpha_s(2\alpha_s^2 - 3)(\alpha_s^2 + 1)^{1/2} + 3\sinh^{-1}\alpha_s), \tag{8}$$

where s stands for $\uparrow$ and $\downarrow$, respectively. From [11]

$$P_{es} + \rho_{es} = n_{es} m_e c^2 \sqrt{\alpha_s^2 + 1}\,. \tag{9}$$

Here, ρ_{es} is the electronic fluid internal energy density. The symbol α_s is the normalized relativistic parameter (ratio of the relativistic *Fermi* momentum and the rest mass momentum of the particle) and is defined as:

$$\alpha_s = \frac{p_{Fes}}{m_e c} = \frac{\hbar}{m_e c}(6\pi^2 n_{es})^{1/3}. \tag{10}$$

At equilibrium, p_{Fes} and n_{es} will be replaced by p_{F0es} and n_{0es}.

From [10], it is clear that the equations of states for both spin species are different due to the presence of applied magnetic field, which causes to change the equilibrium density of each specie $n_{0\uparrow} \neq n_{0\downarrow}$. It is assumed that only one electron of a particular spin can occupy a quantum state (*Pauli Exclusion Principle*). We took $(6\pi^2 n_{0es})^{1/3}$ instead of $(3\pi^2 n_{0es})^{1/3}$ occurring in the *Fermi* momentum state. We have ignored *Bohm* potential in the electron equation according to [22]. At equilibrium, the charge-neutrality condition must be satisfied i.e. $n_{0\uparrow} + n_{0\downarrow} = n_{i0}$.

2.1. Dimensionless evolution equations

Equations (1)–(7), after normalization take the following form:

$$\frac{\partial n_i}{\partial t} + \frac{\partial}{\partial x}(n_i v_{ix}) + \frac{\partial}{\partial z}(n_i v_{iz}) = 0, \tag{11}$$

$$\frac{\partial}{\partial t}\mathbf{v}_i + D\mathbf{v}_i = -\nabla\Phi + \Omega\mathbf{v}_i \times \hat{z}. \tag{12}$$

Here, $D = \mathbf{v}.\nabla$ is the convective derivative

$$\frac{\partial \gamma_\uparrow n_\uparrow}{\partial t} + \frac{\partial}{\partial x}(\gamma_\uparrow n_\uparrow v_{\uparrow x}) + \frac{\partial}{\partial z}(\gamma_\uparrow n_\uparrow v_{\uparrow z}) = 0, \tag{13}$$

$$\frac{\partial \gamma_\downarrow n_\downarrow}{\partial t} + \frac{\partial}{\partial x}(\gamma_\downarrow n_\downarrow v_{\downarrow x}) + \frac{\partial}{\partial z}(\gamma_\downarrow n_\downarrow v_{\downarrow z}) = 0, \tag{14}$$

$$0 = \nabla\Phi - \Omega\mathbf{v}_{e\uparrow} \times \hat{z} - \frac{(1+\kappa)^{2/3}\gamma_\uparrow}{3(\alpha_{0\uparrow}^2 n_\uparrow^{2/3} + 1)} n_\uparrow^{-1/3} \times \left(\nabla + \delta\mathbf{v}_{e\uparrow}\frac{\partial}{\partial t}\right) n_\uparrow, \tag{15}$$

$$0 = \nabla\Phi - \Omega\mathbf{v}_{e\downarrow} \times \hat{z} - \frac{(1-\kappa)^{2/3}\gamma_\downarrow}{3(\alpha_{0\downarrow}^2 n_\downarrow^{2/3} + 1)} n_\downarrow^{-1/3} \times \left(\nabla + \delta\mathbf{v}_{e\downarrow}\frac{\partial}{\partial t}\right) n_\downarrow, \tag{16}$$

$$\frac{\partial^2\Phi}{\partial x^2} + \frac{\partial^2\Phi}{\partial z^2} = \delta_\uparrow\gamma_\uparrow n_\uparrow + \delta_\downarrow\gamma_\downarrow n_\downarrow - \gamma_i n_i. \tag{17}$$

Here, the symbol Φ represents the electrostatic potential ϕ normalized by $\frac{2k_BT_F}{e}$. We have used the definitions $\delta_\uparrow = \frac{n_{0\uparrow}}{n_{i0}}$, $\delta_\downarrow = \frac{n_{0\downarrow}}{n_{i0}}$, $\Omega = \frac{\omega_{ci}}{\omega_{pi}}$, and $\delta = \frac{E_{\rm Fe}}{m_i c^2}$, where Ω is the ion cyclotron frequency $\omega_{ci}\left(=\frac{eB_0}{m_i c}\right)$ normalized by ion plasma frequency $\omega_{pi}(=\sqrt{\frac{4\pi n_{i0}e^2}{m_i}})$ and $E_{\rm Fe}$ represents the electron *Fermi* energy. The ion and electron number densities n_i, $n_\uparrow$ and $n_\downarrow$ are normalized by their corresponding unperturbed values. The velocity $V(=v_i, v_{\uparrow,\downarrow})$ is normalized by the ion-acoustic speed $c_s = \sqrt{\frac{2k_BT_{\rm F}}{m_i}}$ [8]. The spatial and temporal coordinates are normalized by $\lambda_i = \frac{c_s}{\omega_{pi}}$ and inverse of ω_{pi}. The symbol $T_{\rm F}$ represents the electron *Fermi* temperature and is given by $T_F = \frac{(3\pi^2 n_0)^{2/3}\hbar^2}{2k_B m_e}$ [10]. The spin polarization ratio characterizing the spin-up ($n_{e\uparrow}$) and spin-down ($n_{e\downarrow}$) concentrations is defined by the following relation:

$$\kappa = \left(\frac{n_{0\uparrow} - n_{0\downarrow}}{n_{0\uparrow} + n_{0\downarrow}}\right), \quad \kappa \in [0, 1]. \tag{18}$$

By using $\kappa = \frac{\Delta n}{n_0}$ one can get $\delta_\uparrow = \frac{n_{0\uparrow}}{n_{i0}} = \frac{1+\kappa}{2}$, and $\delta_\downarrow = \frac{n_{0\downarrow}}{n_{i0}} = \frac{1-\kappa}{2}$.

3. Linear analysis

We linearize and then *Fourier* analyze the set of equations (11)–(17) by assuming small perturbations to vary

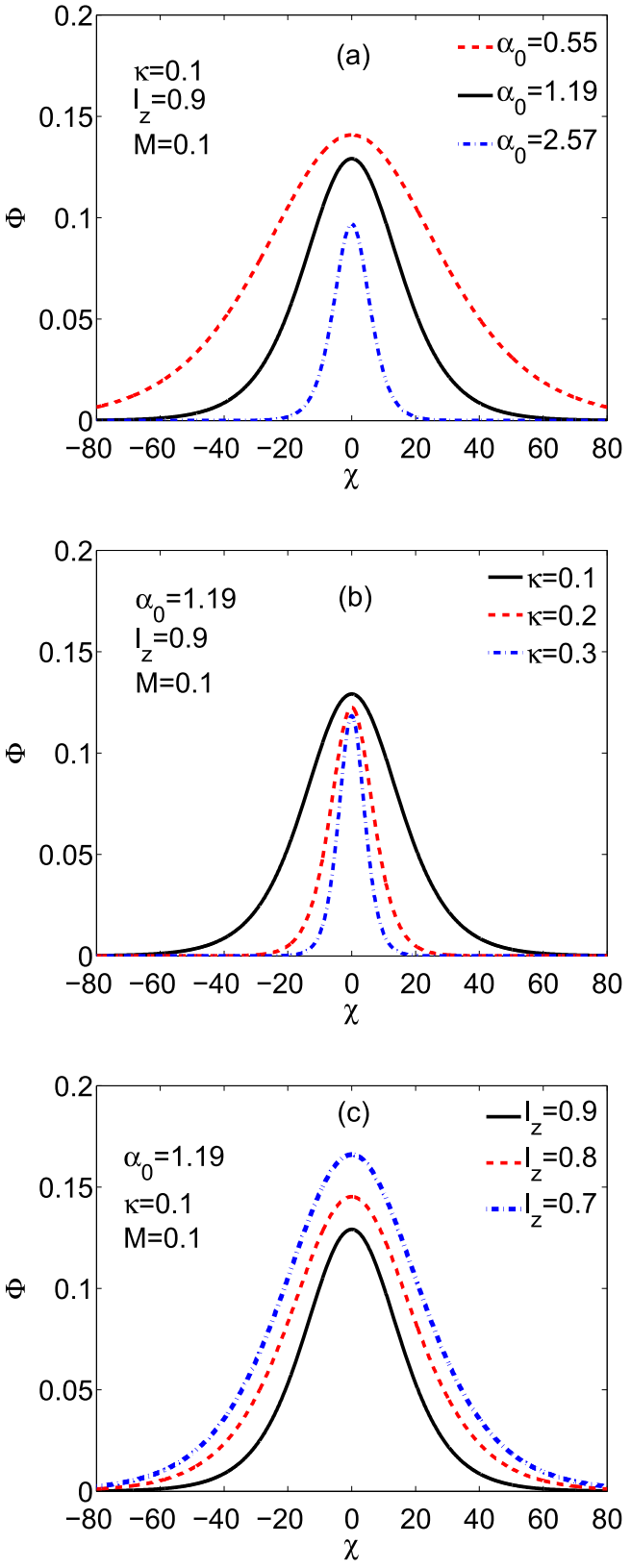

Figure 2. Plot of small amplitude soliton based on equation (31) by using $M = 0.1$. Plots(a) shows the relativistic effect on solitons at $l_z = 0.9$ and $\kappa = 0.1$. Plots (b) depict the variation in the soliton structure with change in the spin polarization for a relativistic plasma at $l_z = 0.9$. The effects of obliqueness on solitons in relativistic plasma with spin polarization $\kappa = 0.1$ for three different values $l_z = 0.9$, $l_z = 0.8$, and $l_z = 0.7$ are plotted in plots (c).

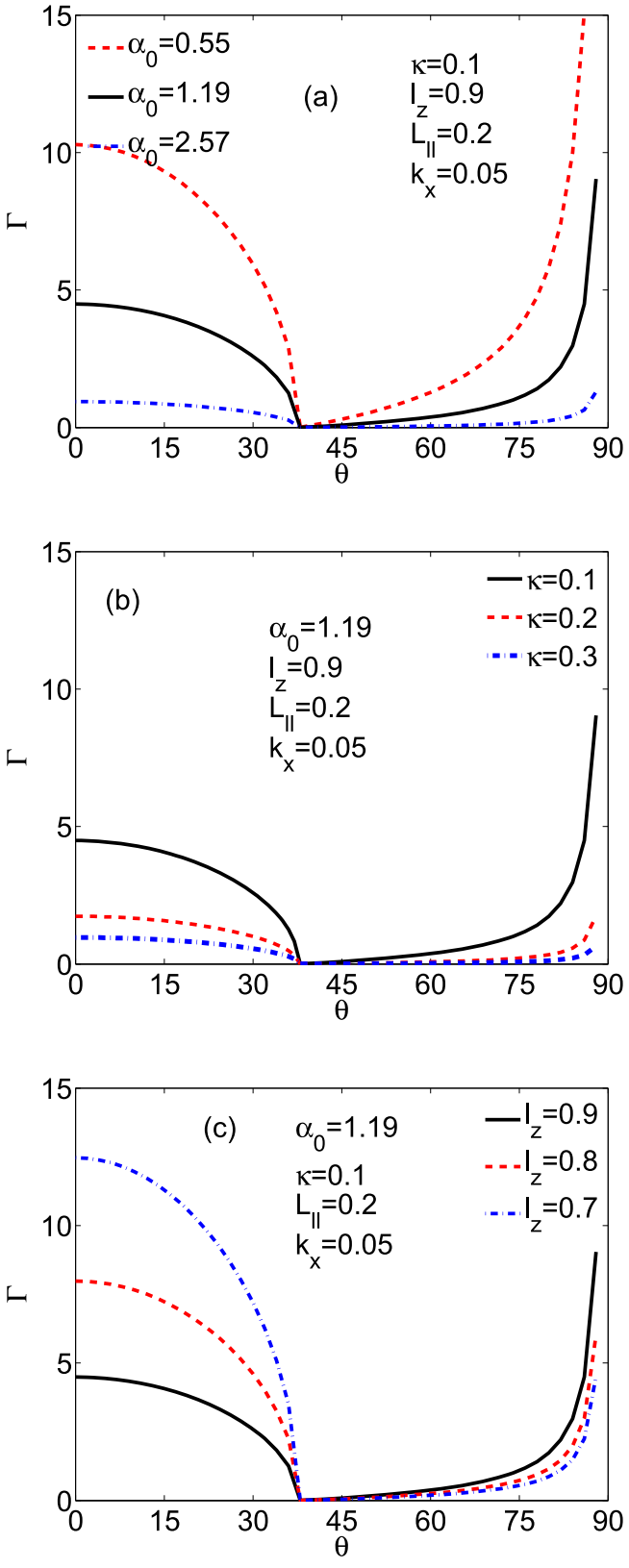

Figure 3. Plots showing the instabilities growth rates Γ_1 and Γ_2 as function of θ for $k_x = 0.05$. Figure (a) shows the relativistic effect on the growth rates of the instability having $\kappa = 0.1$ and $l_z = 0.9$. Figure (b) shows the spin polarization effect κ on the growth rate of the instability in relativistic case, and $L_{\|} = 0.2$, and $l_z = 0.9$. Figure (c) shows plots depicting the effect of l_z on the growth rates of the instability for a relativistic case at $\kappa = 0.1$.

like $\sim e^{i(k_x x + k_z z - \omega t)}$. With some algebraic manipulation, we obtain the following dispersion relation (for detail calculations see appendix A):

$$\omega^4 - b\omega^2 + c = 0, \tag{19}$$

where

$$b = \left[\frac{k^2}{k^2 + \beta} + \Omega^2\right],$$

$$c = \left[\frac{k_z^2 \Omega^2}{k^2 + \beta}\right],$$

$$\beta = \frac{3}{2}[(1+\kappa)^{1/3}(1+\alpha_{0\uparrow}^2) + (1-\kappa)^{1/3}(1+\alpha_{0\downarrow}^2)].$$

Here, the magnitude of the propagation vector is given by $k = \sqrt{(k_x^2 + k_z^2)} = \sqrt{(k_{\|}^2 + k_{\perp}^2)}$. From the above dispersion relation (equation (19)), one can see spin polarization dependence (due to spin-up and spin-down electrons) through the symbol κ. The condition $\kappa = 0$ shows the fact that half of the electrons are spin-up and the remaining half are spin-down, whereas $\kappa = 1$ represents the usual non-polarized electron-ion plasma. The solution of equation (19) is given as:

$$\omega_{\pm}^2 = \left(\frac{b \pm (b^2 - 4c)^{1/2}}{2}\right). \tag{20}$$

It is evident from equation (20) that there is a frequency gap for the upper mode $\omega_+ \to \Omega$ at $k \to 0$ ($k_{\perp} = k_{\|} = 0$) which gives rise to upper-hybrid type of perturbations. Figure 1 is the graphical representation of the dispersion relation (equation (19)). We observe the existence of two modes; low and a high frequency modes for the whole range of $k_{\|}$ except at $k_{\|} = 0$, where the high frequency oscillations exist only. The low frequency mode (ω_-), plotted on the right, is the acoustic oscillations, while the higher frequency mode (ω_+) (plotted on the left) is the *Langmuir*-like mode [23]. The top two plots (a1) and (a2) in figure 1 depict the dispersion of the plasma at three different values of the normalized relativistic parameter of plasma α_0, i.e. $\alpha_0 = 0.55$ for the weakly-relativistic case ($10^{29}\,\mathrm{cm}^{-3}$), $\alpha_0 = 1.19$ for the relativistic case ($10^{30}\,\mathrm{cm}^{-3}$), and $\alpha_0 = 2.57$ representing the ultra-relativistic case ($10^{31}\,\mathrm{cm}^{-3}$). In all these three cases, the spin polarization ratio is kept at $\kappa = 0.1$ and the obliqueness parameter at $k_{\perp} = 0.1$. For the high frequency *Langmuir*-like mode on the left figure 1 (a1), one can see a reduction in both the phase velocity and group velocity as one goes from weakly- relativistic to relativistic and ultra-relativistic case. The phase velocity of the low frequency mode, shown in figure 1 (a2), however, increases as one goes from weakly-relativistic case to ultra-relativistic case. The acoustic mode stops propagating for higher values of $k_{\|}$. In the middle two plots of figure 1, we have kept the obliqueness at $k_{\perp} = 0.1$ for a relativistic plasma and varied the spin polarization ratio by choosing $\kappa = 0.1$, $\kappa = 0.2$, and $\kappa = 0.3$ for both the *Langmuir*-like mode (b1) and the acoustic mode (b2). The spin polarization ratio seems to have a dramatic effect on the propagation of both the modes. For all the three cases of the spin polarization ratio, initially the *Langmuir*-like mode oscillates to some extent of

the $k_{\|}$. The phase velocity during the oscillation increases with increasing polarization ratio and the extent of $k_{\|}$ for which the *Langmuir*-like mode oscillates increases with increasing polarization ratio. During the propagation phase, the group velocity varies inversely with the spin polarization as we go from $\kappa = 0.1$ to $\kappa = 0.2$, and $\kappa = 0.3$. The increasing spin polarization makes the acoustic mode propagate with increasing group velocity to a larger extent of $k_{\|}$. After the extent of $k_{\|}$ when the mode starts oscillating, the phase velocity varies directly with the spin polarization. We have also checked the effect of obliqueness on the propagation of both the *Langmuir*-like and ion-acoustic modes in a relativistic plasma for a spin-polarized case of $\kappa = 0.1$ by varying $k_{\perp}$from $k_{\perp} = 0.1$ to $k_{\perp} = 0.3$ as shown in the bottom plots (c1) and (c2) of figure 1. With initial oscillations to an extent in $k_{\|}$, the *Langmuir*-like mode (c1) propagates with a group velocity that decreases with increasing obliqueness and the phase velocity increases with increasing obliqueness. The lower frequency mode is observed to be propagating initially and then starts oscillating after a fixed value of $k_{\|}$. Both the phase velocity and group velocity reduce with increasing obliqueness. In all cases of interest, the *Langmuir*-like mode has greater speed than the acoustic and hence the term fast and slow mode respectively.

4. Nonlinear analysis

To study the nonlinear properties of the IAWs (solitary structures) in the magnetized quantum plasma containing spin-up ($n_{e\uparrow}$) and spin-down ($n_{e\downarrow}$) as two different species of relativistic degenerate electrons, the standard procedure of RPT [24] has been used to obtain the ZK equation. We have taken $\nabla = (\partial_x, 0, \partial_z)$. We have stretched the spatial and temporal variables as: $X = \epsilon^{1/2}x$, and $Z = \epsilon^{1/2}(z - v_p t)$ and $T = \epsilon^{3/2}t$, where the symbol ϵ represents the strength of nonlinearity and v_p is the normalized waves speed. We have expanded the dynamical quantities by following the procedure used in [25] as below:

$$n_i \simeq 1 + \epsilon n_i^{(1)} + \epsilon^2 n_i^{(2)} + \epsilon^3 n_i^{(3)} \cdots, \tag{21}$$

$$n_{\uparrow,\downarrow} \simeq 1 + \epsilon n_{\uparrow,\downarrow}^{(1)} + \epsilon^2 n_{\uparrow,\downarrow}^{(2)} + \epsilon^3 n_{\uparrow,\downarrow}^{(3)} \cdots, \tag{22}$$

$$v_z \simeq \epsilon v_z^{(1)} + \epsilon^2 v_z^{(2)} + \epsilon^3 v_z^{(3)} \cdots, \tag{23}$$

$$v_{x,y} \simeq \epsilon^{3/2} v_{x,y}^{(1)} + \epsilon^2 v_{x,y}^{(2)} + \epsilon^{5/2} v_{x,y}^{(3)} \cdots, \tag{24}$$

$$\Phi \simeq \epsilon \Phi^{(1)} + \epsilon^2 \Phi^{(2)} + \epsilon^3 \Phi^{(3)} \cdots. \tag{25}$$

By putting the above expansions into the dynamical equations (equations (11)–(17)) and comparing the coefficients of the lowest powers ($\sim\varepsilon$), we obtain phase velocity v_p

$$v_p = \sqrt{\frac{2}{3((1+\kappa)^{1/3}(1+\alpha_{0\uparrow}^2) + (1-\kappa)^{1/3}(1+\alpha_{0\downarrow}^2))}}, \tag{26}$$

for detail calculations see appendix B.

Separating the next higher order quantities, we get the ZK equation, which is given as:

$$\frac{\partial \Phi}{\partial T} + A\Phi\frac{\partial \Phi}{\partial Z} + \frac{\partial}{\partial Z}\left(B\frac{\partial^2 \Phi}{\partial Z^2} + C\frac{\partial^2 \Phi}{\partial X^2}\right) = 0. \tag{27}$$

Here, $\Phi = \Phi^{(1)}$ has been used for simplicity. In the ZK equation (27), the real coefficients A (nonlinear coefficient), B and C (dispersion coefficients) have the following explicit values:

$$\begin{aligned} A \;=\; & \frac{v_p^3}{2}\left(\frac{3}{v_p^4} - \frac{3}{2}\frac{(1+\alpha_{0\uparrow}^2)(1+3\alpha_{0\uparrow}^2)}{(1+\kappa)^{1/3}}\right. \\ & - \frac{3}{2}\frac{(1+\alpha_{0\downarrow}^2)(1+3\alpha_{0\downarrow}^2)}{(1-\kappa)^{1/3}} + \frac{\delta}{v_p^2} \\ & \left. - \frac{9\delta v_p^2(1+\alpha_{0\downarrow}^2)^2}{(1-\kappa)^{1/3}} - \frac{9\delta v_p^2(1+\alpha_{0\uparrow}^2)^2}{(1+\kappa)^{1/3}}\right), \end{aligned} \tag{28}$$

$$B = \frac{v_p^3}{2}, \tag{29}$$

$$C = \frac{v_p^3}{2}(1 + \Omega^{-2}). \tag{30}$$

For detail calculations see appendix C. Equation (27) is the ZK equation governing the nonlinear evolution of the acoustic waves which are obliquely propagating in a magnetized quantum plasma having both spin-up ($n_{e\uparrow}$) and spin-down ($n_{e\downarrow}$) populations of relativistic degenerate electrons and relativistic classical ions.

4.1. Solitary wave solution

To solve the ZK equation (equation (27)) analytically for a single pulse, we use the well-known *tanh-method* [26]. We use the transformation $\xi = \chi(l_x X + l_z Z - MT)$, where M represents the soliton velocity moving with the frame, χ has the dimension of inverse of soliton's width and l_x, l_z are the direction cosines of the propagation wave vector $\mathbf{k}$ along X and Z directions, respectively. Hence, $l_x^2 + l_z^2 = 1$. The important fact to be noted here is that the ansatz deals only with the oblique propagation with respect to the applied magnetic field ($\theta = \tan^{-1}(l_x/l_z)$), whereas it breaks down for the purely transverse propagation ($l_z = 0$) [27]. By using *tanh-method*, the solitary wave solution of equation (27) is given as:

$$\Phi = \Phi_m \,\mathrm{sech}^2(\xi). \tag{31}$$

Details on the algebraic procedure can be found in appendix A of [28]. In the equation (31), $\Phi_m = \frac{3M}{l_z A}$ is the amplitude of the soliton, $\xi = \chi(l_x X + l_z Z - MT)$ and $\chi^{-1} = \sqrt{\frac{4l_x(Bl_z^2 + Cl_x^2)}{M}}$ is the width of the soliton. It is clear that the amplitude of solitons depends upon the nonlinear coefficient whereas the width of soliton is the function of dispersive coefficients. In this study, it has been found that the present model admits only compressive solitons for the plasma parameters studied in this article.

We have plotted the solution of equation (31) in figure 2 by varying the electron density and accessed three different plasma regimes; weakly-relativistic ($10^{29}\,\mathrm{cm}^{-3}$), relativistic ($10^{30}\,\mathrm{cm}^{-3}$), and ultra-relativistic ($10^{31}\,\mathrm{cm}^{-3}$). As can be seen from plots in figure 2(a), at the spin polarization value $\kappa = 0.1$ and the obliqueness $l_z = 0.9$, both the width and amplitude of the acoustic solitons decrease as we move from the weakly relativistic regime to the ultra-relativistic regime. Figure 2(b) shows the effect of spin polarization on the structure of solitons in a relativistic case at an obliqueness value of $l_z = 0.9$. The obliqueness value of $l_z = 0.9$ is chosen only to make a representative case. We observe that the width of the soliton decreases with increase in the value of the polarization parameter κ. The amplitude remains largely unchanged with variation in the spin polarization. The choice of the polarization parameter $\kappa = 0.1,\ 0.2,\ 0.3$ is only for demonstrating the effect of polarization. We also studied the effect of propagation direction via l_z on the amplitude and width of the nonlinear structures. As explained by Verheest [29], one needs to keep the angle between propagation vector $\mathbf{k}$ and the applied magnetic field $\mathbf{B}_0$ as small to satisfy the criteria for electrostatic approximation. It is observed (see figure 2(c)) that for the relativistic plasma with spin polarization $\kappa = 0.1$, both the amplitude and width of the solitons increase with decrease in the value of l_z from 0.9 to 0.7. Once again, the choice-values of l_z amply demonstrate the changes in the soliton structures with the obliqueness parameter.

5. Stability analysis

In this section, we investigate the stability of the solitary wave solution of equation (31) by using the procedure developed in [30]. By using proper scaling i.e. $\Phi \to \Phi_0\hat{\Phi}$, $T \to T_0T'$, $Z \to L_\parallel Z'$, $X \to L_\perp X'$: the ZK-equation (equation (27)) is converted to 'canonical' form as:

$$\frac{\partial\hat{\Phi}}{\partial\acute{T}} + \hat{\Phi}\frac{\partial\hat{\Phi}}{\partial\acute{Z}} + \frac{\partial}{\partial\acute{Z}}\left(\frac{\partial^2\hat{\Phi}}{\partial^2\acute{Z}} + \frac{\partial^2\hat{\Phi}}{\partial^2\acute{X}}\right) = 0. \tag{32}$$

This canonical equation has a form similar to equation (1.1) appeared in [30]. Here we focus mainly on the salient features of the instability instead of its re-derivation. For details, the readers may consult the articles by Allen and Rowlands [30], and Adnan *et al* [31].

The solution of equation (32) is

$$\hat{\Phi} = \Phi_0 + \epsilon\,\Phi(x)\mathrm{e}^{\mathrm{i}k_x x}\mathrm{e}^{\gamma t}. \tag{33}$$

Here, Φ_0 represents the equilibrium solution of equation (32), γ is the instability growth rate, and k_x is the transverse component of the propagation vector. The function $\Phi\ (x)$ is calculated by using the multi-scale perturbation, depending on an expansion in the magnitude of the wave vector $\mathbf{k}$ [30].

In the small k limits, the instability growth rate (Γ) is directly proportional to the real part of γ [30], and is expressed as

$$\Gamma = k\gamma_1 + k^2\gamma_2 + \ldots\ldots. \tag{34}$$

Here, γ_1 and γ_2 represent the first and second order instabilities respectively. By performing a detailed calculation [30–32], we get the following expression for the first order instability:

$$\gamma_1 = \frac{8}{3}\left[\left(\frac{8}{5}\cos^2\theta - 1\right)^{\frac{1}{2}} + \mathrm{i}\sin\theta\right]. \tag{35}$$

Here, θ is the angle made by perpendicular component of propagation vector and the externally applied magnetic field. The expression $\left(\frac{8}{5}\cos^2\theta - 1\right)^{\frac{1}{2}} < 0$ leads to $\theta < 37.8^\circ$ for γ_1 to occur.

It may be noted that the second order instability which is $\sim k^2$ may even takes place if the system is stable to the first order ($\sim k$). The second order instability growth rate has the following mathematical form:

$$\gamma_2 = -\frac{4}{9}\left[\left(\frac{8}{5}\cos^2\theta - 1\right)\sec\theta + \frac{4(5 + 4\cos^2\theta)\mathrm{i}\tan\theta}{45\left(\frac{8}{5}\cos^2\theta - 1\right)^{\frac{1}{2}}}\right]. \tag{36}$$

The Allen-Rowlands analysis [30] is summarized as follow:

(1) For $\theta < \theta_{cr} \simeq 37.8^\circ$ the instability growth rate is

$$\Gamma_1 = kRe(\gamma_1) + O(k^2) \simeq k\frac{8}{3}\left(\frac{8}{5}\cos^2\theta - 1\right)^{\frac{1}{2}}. \tag{37}$$

(2) For $\theta > \theta_{cr} \simeq 37.8^\circ$, the instability growth rate is

$$\Gamma_2 = kRe(\gamma_1) + O(k^3) \simeq -k^2\frac{4}{9}\left(\frac{8}{5}\cos^2\theta - 1\right)\sec\theta. \tag{38}$$

To go back to our original model by using the transformation $\Phi_0 = \frac{B}{L_\parallel^2 A}$, $T_0 = \frac{L_\parallel^3}{B}$, $L_\parallel \in \Re$ and $L_\perp = L_\parallel\left(\frac{C}{B}\right)^{\frac{1}{2}}$ for Φ, time, z and x respectively, we get equations (37) and (38) in the corresponding dimensional variables as:

$$\Gamma_1 \simeq k\frac{(BC)^{\frac{1}{2}}}{L_\parallel^2}\frac{8}{3}\left(\frac{8}{5}\cos^2\theta - 1\right)^{\frac{1}{2}} \tag{39}$$

and

$$\Gamma_2 \simeq -k^2\frac{C}{L_\parallel}\frac{4}{9}\left(\frac{8}{5}\cos^2\theta - 1\right)\sec\theta. \tag{40}$$

Here, we have used the scaling $k \longrightarrow kL_\perp$, $\gamma_1 \longrightarrow \gamma_1 T_0$ and $\gamma_2 \to \gamma_2 T_0$.

We have parametrically investigated the dependence of the first order instability growth rate Γ_1 as well as the second order instability growth rate Γ_2 on plasma parameters such as the relativistic degeneracy factor α, spin polarization κ and obliqueness l_z by employing equations (39) and (40). In all cases the first order instability growth rate Γ_1 reduces to zero at $\theta = \theta_{cr} = 37.8^\circ$. Beyond θ_{cr}, Γ_2 sees an abrupt increase. In figure 3(a), we have plotted the growth rates Γ_1 and Γ_2 against θ by varying the relativistic degeneracy factor at $\kappa = 0.1$ and $l_z = 0.9$ for $k_x = 0.05$. We observe a reduction in the growth rates of the instability as we move from weakly relativistic

regime to ultra-relativistic regime. For the relativistic regime, we varied the spin polarization κ at $L_{\|} = 0.2$, and $l_z = 0.9$ and we see (figure 3(b)) that the spin polarization significantly reduces the growth rates, especially the second order instability. We also studied the effect of obliqueness on the growth rates of the instability in the relativistic regime studied above for $L_{\|} = 0.2$, and $\kappa = 0.1$. A drastic enhancement in the growth rate is observed as the value of l_z is reduced from 0.9 to 0.8 and 0.7 for the smaller angles θ. For $\theta > 37.8°$, the effect of the obliqueness on the growth rate of the second order instability is not very significant.

6. Conclusions

We have investigated the propagation of low frequency acoustic waves in magnetized quantum plasma consisting of inertia-less relativistic degenerate electrons having both spin up ($n_{e\uparrow}$) and the spin down ($n_{e\downarrow}$) concentrations and relativistic non-degenerate dynamical ions. We have investigated both linear and nonlinear waves by taking the degenerate electrons having spin up ($n_{e\uparrow}$) and spin down ($n_{e\downarrow}$) states as two different species. In the linear regime we got two dispersion curves that correspond to two different modes; a slow (acoustic) mode and a fast (*Langmuir*-like) mode. Our results indicate that in all cases of interest, from weakly-relativistic to ultra-relativistic cases at the spin polarization value of $\kappa = 0.1$, barring the initial increment in $k_{\|}$, the phase speed decreases with increase in density of the system. Furthermore, while the *Langmuir*-like mode (fast-mode) propagates for the most part of the investigation, the slow-mode (acoustic) starts oscillating after the initial brief propagation. The increasing spin polarization enhances the phase speed of the slow mode but the effect is limited to the initial values of $k_{\|}$ in case of the *Langmuir*-like mode where the effect reverses after some propagation. The obliqueness has been shown to favor the *Langmuir*-like mode while it depresses the slow mode.

The solution of our ZK-type equation provides localized solitary structures that are only compressive in nature. A reduction in both the width and amplitude of the solitons has been observed as one goes from weakly-relativistic regime to ultra-relativistic regime. The width of the solitons has been observed to be inversely proportional to the polarization density. An increase in both the amplitude and width of the solitons with a reduction in the direction ratio l_z has also been observed.

From the instability analysis, it can be seen that the first order instability growth rate (γ_1) decreases with θ (i.e. the angle between the perpendicular component of the propagation vector and the direction of the ambient magnetic field) in the range ($0 \leqslant \theta < 37.8^0$). A decrease in the growth rate is also recorded by changing the spin polarization ratio from 0.1 to 0.3 and by varying the normalized relativistic parameter of plasma α_0. Furthermore, the second order instability growth rate (γ_2) increases sharply beyond $\theta > 37.8$ and attains saturation at larger values of θ inversely with spin polarization ratio and relativistic effects.

Appendix A. Derivation of the dispersion relation

Replacing $\frac{\partial}{\partial t}$ by $-\mathrm{i}\omega$, $\frac{\partial}{\partial x}$ by $\mathrm{i}k_x$, and $\frac{\partial}{\partial z}$ by $\mathrm{i}k_z$, equation (12) gives

$$v_{iy}^{(1)} = -\mathrm{i}\frac{\Omega}{\omega}v_{ix}^{(1)}, \quad v_{ix}^{(1)} = \frac{k_x\omega}{(\omega^2 - \Omega^2)}\Phi^{(1)},$$
$$v_{iz}^{(1)} = \frac{k_z}{\omega}\Phi^{(1)}. \tag{A.1}$$

By substituting the above values in equation (11), we obtain the ion number density in terms of $\Phi^{(1)}$

$$n_i^{(1)} = \left(\frac{{k_x}^2}{\omega^2 - \Omega^2} + \frac{{k_z}^2}{\omega^2}\right)\Phi^{(1)}. \tag{A.2}$$

Similarly from equations (15) and (16), we obtain electron number densities in terms of $\Phi^{(1)}$

$$n_\uparrow^{(1)} = \frac{3({\alpha_0}_\uparrow{}^2 + 1)}{(1 + \kappa)^{2/3}}\Phi^{(1)}, \quad n_\downarrow^{(1)} = \frac{3({\alpha_0}_\downarrow{}^2 + 1)}{(1 - \kappa)^{2/3}}\Phi^{(1)}. \tag{A.3}$$

Substituting the values of $n_i^{(1)}$, $n_\uparrow^{(1)}$ and $n_\downarrow^{(1)}$ in equation (17) we obtain equation (19).

Appendix B. First order perturbed quantities and phase velocity

By putting the expansions (22)–(26) into the dynamical equations (11)–(17) and comparing the coefficients of the lowest powers ($\sim\varepsilon^{3/2}$), we obtain:

$$\frac{\partial n_i^{(1)}}{\partial Z} = \frac{1}{v_p^2}\frac{\partial\Phi^{(1)}}{\partial Z}, \quad \frac{\partial v_{iz}^{(1)}}{\partial Z} = \frac{1}{v_p}\frac{\partial\Phi^{(1)}}{\partial Z}, \tag{B.1}$$

$$\frac{\partial n_{1\uparrow}^{(1)}}{\partial Z} = \frac{3(1 + \alpha_{0\uparrow}^2)}{(1 + \kappa)^{2/3}}\frac{\partial\Phi^{(1)}}{\partial Z}, \tag{B.2}$$

$$\frac{\partial n_{1\downarrow}^{(1)}}{\partial Z} = \frac{3(1 + \alpha_{0\uparrow}^2)}{(1 - \kappa)^{2/3}}\frac{\partial\Phi^{(1)}}{\partial Z}, \tag{B.3}$$

$$\frac{\partial v_{z1\uparrow}^{(1)}}{\partial Z} = \frac{3v_p(1 + \alpha_{0\uparrow}^2)}{(1 + \kappa)^{2/3}}\frac{\partial\Phi^{(1)}}{\partial Z}, \tag{B.4}$$

$$\frac{\partial v_{z1\downarrow}^{(1)}}{\partial Z} = \frac{3v_p(1 + \alpha_{0\uparrow}^2)}{(1 - \kappa)^{2/3}}\frac{\partial\Phi^{(1)}}{\partial Z}, \tag{B.5}$$

$$v_{ix}^{(1)} = 0, \quad v_{iy}^{(1)} = \frac{1}{\Omega}\frac{\partial\Phi^{(1)}}{\partial X}, \tag{B.6}$$

$$\left(\frac{1 + \kappa}{2}\right)n_{e\uparrow}^{(1)} + \left(\frac{1 - \kappa}{2}\right)n_{e\downarrow}^{(1)} - n_i^{(1)} = 0. \tag{B.7}$$

Taking derivative of equation (B.7) with respect to Z we get

$$\left(\frac{1 + \kappa}{2}\right)\frac{\partial n_{e\uparrow}^{(1)}}{\partial Z} + \left(\frac{1 - \kappa}{2}\right)\frac{\partial n_{e\downarrow}^{(1)}}{\partial Z} - \frac{\partial n_i^{(1)}}{\partial Z} = 0. \tag{B.8}$$

Putting $\frac{\partial n_i^{(1)}}{\partial Z}$, $\frac{\partial n_\uparrow^{(1)}}{\partial Z}$ and $\frac{\partial n_\downarrow^{(1)}}{\partial Z}$ in equation (B.8) we obtain the expression for the phase velocity equation (26).

Appendix C. Second order perturbed quantities and ZK equation

Separating the next higher order quantities, we get

$$-v_p\frac{\partial n_i^{(2)}}{\partial Z}+\frac{\partial n_i^{(1)}}{\partial T}+\frac{\partial v_{ix}^{(2)}}{\partial X}+\frac{\partial v_{iz}^{(2)}}{\partial Z}+\frac{\partial}{\partial Z}(n_i^{(1)}v_{iz}^{(1)})=0, \tag{C.1}$$

$$-v_p\frac{\partial v_{iz}^{(2)}}{\partial Z}+\frac{\partial v_{iz}^{(1)}}{\partial T}+v_{iz}^{(1)}\frac{\partial v_{iz}^{(1)}}{\partial Z}+\frac{\partial \Phi^{(2)}}{\partial Z}=0, \tag{C.2}$$

$$\frac{\partial n_\uparrow^{(2)}}{\partial Z}=\left(\frac{3(1+\alpha_{0\uparrow}^2)(1+3\alpha_{0\uparrow}^2)}{(1+\kappa)^{4/3}}+\frac{9\delta v_p^2(1+\alpha_{0\uparrow}^2)^2}{(1+\kappa)^{4/3}}\right)\Phi^{(1)}\frac{\partial\Phi^{(1)}}{\partial Z}, \tag{C.3}$$

$$\frac{\partial n_\downarrow^{(2)}}{\partial Z}=\left(\frac{3(1+\alpha_{0\downarrow}^2)(1+3\alpha_{0\downarrow}^2)}{(1-\kappa)^{4/3}}+\frac{9\delta v_p^2(1+\alpha_{0\downarrow}^2)^2}{(1-\kappa)^{4/3}}\right)\Phi^{(1)}\frac{\partial\Phi^{(1)}}{\partial Z}, \tag{C.4}$$

$$v_{iy}^{(2)}=0,\quad v_{ix}^{(2)}=\frac{v_p}{\Omega^2}\frac{\partial\Phi^{(1)}}{\partial Z\partial X}, \tag{C.5}$$

$$\frac{\partial^2\Phi^{(1)}}{\partial X^2}+\frac{\partial^2\Phi^{(1)}}{\partial Z^2}=\left(\frac{1+\kappa}{2}\right)n_\uparrow^{(2)}+\left(\frac{1-\kappa}{2}\right)n_\downarrow^{(2)}-n_i^{(2)}+\delta\left(\frac{1+\kappa}{4}\right)v_{z\uparrow}^{(1)^2}+\delta\left(\frac{1-\kappa}{4}\right)v_{z\downarrow}^{(1)^2}-\frac{\delta}{2}v_{iz}^{(1)^2}. \tag{C.6}$$

For the derivation of equation (27) taking the derivative of equation (C.6) with respect to Z,

$$\frac{\partial^3\Phi^{(1)}}{\partial Z\partial X^2}+\frac{\partial^3\Phi^{(1)}}{\partial Z^3}=\left(\frac{1+\kappa}{2}\right)\frac{\partial n_\uparrow^{(2)}}{\partial Z}+\left(\frac{1-\kappa}{2}\right)\frac{\partial n_\downarrow^{(2)}}{\partial Z}-\frac{\partial n_i^{(2)}}{\partial Z}+\delta\left(\frac{1+\kappa}{2}\right)v_{z\uparrow}^{(1)}\frac{\partial v_{z\uparrow}^{(1)}}{\partial Z}+\delta\left(\frac{1-\kappa}{2}\right)v_{z\downarrow}^{(1)}\frac{\partial v_{z\downarrow}^{(1)}}{\partial Z}-\delta v_{iz}^{(1)^2}\frac{\partial v_{iz}^{(1)}}{\partial Z}. \tag{C.7}$$

Putting the values of $\frac{\partial n_i^{(2)}}{\partial Z}$, $\frac{\partial n_\uparrow^{(2)}}{\partial Z}$, $\frac{\partial n_\downarrow^{(2)}}{\partial Z}$, $v_{iz}^{(1)}$, $v_{\uparrow z}^{(1)}$, $v_{\downarrow z}^{(1)}$, $\frac{\partial v_{iz}^{(1)}}{\partial Z}$, $\frac{\partial v_{z\uparrow}^{(1)}}{\partial Z}$ and $\frac{\partial n_{z\downarrow}^{(1)}}{\partial Z}$ we get the ZK equation (equation (27)).

ORCID iDs

Rashid Ahmad https://orcid.org/0000-0001-5945-0549
Fida Younus Khattak https://orcid.org/0000-0002-0270-6766

References

[1] Shapiro S L and Teukolsky S A 2004 *Black Holes, White Dwarfs, and Neutron Stars—The Physics of Compact Objects* (Weinheim: Wiley-VCH)
[2] Lai D 2001 *Rev. Mod. Phys.* **73** 629
[3] Fortov V E, Lakubov I T and Khrapak A G 2006 *Physics of Strongly Coupled Plasma* (Clarendon: Oxford)
[4] Yalabik M C, Neofotistos G, Diff K, Guo H and Gunton J 1989 *IEEE Trans. Electron Devices* **36** 1009
[5] Bigot J Y, Merle J Y, Cregut O and Daunois A 1995 *Phys. Rev. Lett.* **75** 4702
[6] Moses E I, Boyd R N, Remington B A, Keane C J and Al-Alayat R 2009 *Phys. Plasmas* **16** 041006
[7] Glenzer S H *et al* 2007 *Phys. Rev. Lett.* **98** 065002
[8] Haas F, Garcia L G, Goudert G and Manfredi G 2003 *Phys. Plasmas* **10** 3858
[9] Marklund M 2005 *Phys. Plasmas* **12** 082110
[10] Andreev P A 2015 *Phys. Rev.* E **91** 033111
[11] Behery E E, Haas F and Kourakis I 2016 *Phys. Rev.* E **93** 023206
[12] Zou J P *et al* 2015 *High Power Laser Sci. Eng.* **3**
[13] Salpeter E E 1961 *Astrophys. J.* **134** 669
[14] Chandrasekhar S 1931 *Phil. Mag.* **11** 591
[15] Chandrasekhar S 1931 *Astrophys. J.* **74** 81
[16] Russo G 1988 *Astrophys. J.* **334** 707
[17] McKerr M, Haas F and Kourakis I 2014 *Phys. Rev.* E **90** 033112
[18] Manfredi G 2005 *Fields Inst. Commun. Ser.* **46** 263
[19] Brodin G, Marklund M, Zamanian J and Stefan M 2011 *Plasma Phys. Control. Fusion* **53** 074013
[20] Andreev P A and Kuzmenkov L S 2015 *Ann. Phys.* **361** 278
[21] Ahmad R, Gul N, Adnan M and Khattak F Y 2016 *Phys. Plasmas* **23** 112112
[22] Haas F and Eliassos B 2015 *Phys. Scr.* **90** 088005
[23] Trivelpiece A W and Gould A W 1959 *J. Appl. Phys.* **30** 1784
[24] Washimi H and Taniuti T 1966 *Phys. Rev. Lett.* **17** 996
[25] Rowlands G 1969 *J. Plasma Phys.* **3** 567
[26] Malfliet W 2004 *J. Comput. Appl. Math.* **164** 529
[27] Kourakis I, Moslem W M, Abdelsalam U M, Sabry R and Shukla P K 2009 *Plasma Phys. Control. Fusion* **4** 018
[28] Williams G and Kourakis I 2013 *Plasma Phys. Control. Fusion* **55** 055005
[29] Verheest F 2009 *J. Phys. A: Math. Theor.* **42** 285501
[30] Allen M A and Rowlands G 1995 *J. Plasma Phys.* **53** 63
[31] Adnan M, Williams G, Qamar A, Mahmood S and Kourakis I 2014 *Eur. Phys. J.* D **68** 247
[32] Williams G and Kourakis I 2013 *Phys. Plasmas* **20** 122311